SUPPLEMENTAL DATA

1. Synthesis of [^{18}F]PFPMD and its corresponding Nonradioactive PFPMD.

Compound 2: *2-(2-(2-(2-fluoroethoxy)ethoxy)ethoxy)ethyl 4-methylbenzenesulfonate*. A mixture of ((oxybis(ethane-2,1-diyl))bis(oxy))bis(ethane-2,1-diyl) bis(4-methylbenzenesulfonate) (compound **1**, 1.05 g, 2.09 mmol), Tetrabutylammonium fluoride (TBAF, 0.55 g, 2.10 mmol), K_2CO_3 (0.89 g, 6.44 mmol), and trace KI in acetonitrile (2 mL) was stirred at 90 °C for 12 h. The product was separated by HPLC and freeze-dried overnight to obtain a yellow oil (0.51mg, 69.6 %).

F-PFMP: *4-((S)-4-acryloyl-2-methylpiperazin-1-yl)-6-fluoro-7-(2-fluoro-6-(2-(2-(2-(2-fluoroethoxy)ethoxy)ethoxy)ethoxy)phenyl)-1-(2-isopropyl-4-methylpyridin-3-yl)pyrido[2,3-d]pyrimidin-2(1H)-one.* AMG510 (26.2 mg, 0.047 mmol) was dissolved in 0.2 ml of anhydrous DMSO and add 0.8 ml of acetonitrile solution of compound **2** (27.6 mg, 0.079 mmol) to form a pale yellow clear solution. After the addition of anhydrous potassium carbonate (25.9 mg, 0.19 mmol), the solution deepened in yellow and refluxed for 12 hours. The product was obtained by HPLC and freeze-dried overnight to give a white powder (13.8 mg, 39.8%).

PPMD-OTs: *2-(2-(2-(2-(2-(4-((S)-4-acryloyl-2-methylpiperazin-1-yl)-6-fluoro-1-(2-isopropyl-4-methylpyridin-3-yl)-2-oxo-1,2-dihydropyrido[2,3-d]pyrimidin-7-yl)-3-fluorophenoxy)ethoxy)ethoxy)ethoxy)ethyl 4-methylbenzenesulfonate*

The procedure described for the synthesis of Compound **2** was applied to compound 1 (68.0 mg, 0.14 mmol) and AMG510 (40.6 mg, 0.072 mmol) to afford tosylate precursor PPMD-OTs as a white solid (21.0

mg, 32.6%).

[^{18}F]PFPMD: Radiolabeling was prepared by AllinOne universal synthesizer (Trasis, Belgium) (Supplemental Figure 1). [^{18}F]Fluoride was produced *via* the ^{18}O (p,n) ^{18}F reaction by Cyclone (SUMITOMO HM-12) at Xi'an PET Tracer Co., Ltd. (Xi'an, China). Aqueous [^{18}F]fluoride (300 mCi, 2.5 mL) was passed through a resin cartridge (QMA) where the [^{18}F]fluoride was trapped. [^{18}F]Fluoride was eluted using a mixture of Kryptofix2.2.2 (8 mg, 22.9 μmol), anhydrous potassium carbonate (1 mg, 7.2 μmol), in acetonitrile (0.80 mL) and water (0.20 mL). The solvent was removed by azeotropic drying at 120 °C under a stream of nitrogen. After cooling to 60 °C, a solution of the tosylate precursor (AMG510-OTs, 2 mg) in anhydrous acetonitrile (1.0 mL) was added. The reaction mixture was incubated at 100 °C for 10 minutes to provide [^{18}F]PFPMD. Diluted with water and trapped on a Waters C18 plus Sep-Pak cartridge. The product was eluted off the cartridge with anhydrous acetonitrile. Loaded onto a sample loop in the isocratic semi-preparative radio-HPLC for purification (Agela Venusil MP C18 column, 250 mm × 10 mm, 5 μm, eluent 42% CH_3CN and 58% H_2O, flow rate 4 mL/min). The product peak was collected, diluted with water and trapped on a Waters C18 light Sep-Pak cartridge. The cartridge was washed with water. The product was eluted off the cartridge with ethanol and filtrated by Millex-GV filter (0.22 μm). Radiochemical purity was analyzed by analytical radio-HPLC using a different C18 column (Agela Venusil MP C18 column, 250 mm × 4.6 mm, 5 μm, gradient eluent CH_3CN and H_2O containing 0.1% TFA, the CH_3CN was maintained at 5% from 0-5 min, then increased to 65% at 12 min and maintained until 20 min, flow rate 1 mL/min). For experiments, [^{18}F]PFPMD was formulated as a saline solution containing no more than 10% ethanol.

2. Determination of chemical purity

Chemical purity was analyzed by analytical HPLC using a C18 column (Agela Venusil MP C18 column, 250 mm × 4.6 mm, 5 μm, gradient eluent CH_3CN and H_2O containing 0.1% TFA, the CH_3CN was maintained at 5% from 0-5 min, then increased to 65% at 12 min and maintained until 20 min, flow rate 1 mL/min).

3. Determination of molar activity.

0.4, 2, 10, 20, 33.3 μg of the corresponding nonradioactive compound F-PFMP was dissolved in 10% acetonitrile and the UV absorption peak areas were determined by HPLC and repeated three times, respectively. The standard curve (Supplemental Figure 6) was made with the amount of substance as the horizontal coordinate and the peak area as the vertical coordinate, and the linear equation of the standard curve was obtained as follows: $y = 220.73x + 95.89$, $R^2 = 0.9998$. The UV absorption peak area of [^{18}F]PFPMD was measured as y. And x, the amount of substance of [^{18}F]PFPMD, was calculated from the linear equation of the standard curve. Finally, the molar activity was calculated based on the activity corresponding to [^{18}F]PFPMD.

4. Determination of log D value.

The distribution coefficient of [^{18}F]PFPMD was determined by measuring the distribution of the radiotracer between 1-octanol and potassium phosphate buffer (PBS, 0.05 mol/L, pH 7.4). The radiotracer (10 μL, 1100 kBq) was mixed with 1-octanol (3 mL) and potassium phosphate buffer (3 mL) in a centrifuge tube (15 mL). The tube was vortexed for 3 min, followed by centrifugation at 3500 rpm for 5 min (Cence L500-A, China). About 0.05 mL of 1-octanol layer was weighed in a tared tube. About 0.5 mL of the PBS layer was weighed in a second tared tube. The activity in both tubes was measured in an automatic γ-counter (WIZARD 2470, PerkinElmer, USA). The log D value was calculated as the ratio of the cpm/mL of 1-octanol to that of PBS and expressed as log D = log [cpm/mL(1-octanol)/cpm/mL(PBS)]. Samples from the remaining organic layer were repartitioned until consistent distribution coefficient values were obtained. The measurement was carried out in triplicate and repeated three times.

5. Molecular docking.

Molecular docking was conducted in Molecular Operating Environment (MOE) v2018.01. The 2D structures of cpd1 was prepared by molecule and protein build module in MOE and converted to 3D structure through energy minimization. The reactive covalent site was Cys12 for KRAS G12C. The covalent reaction was defined in Marvin Sketch, the sidechain sulfur atom was the nucleophilic reactive site and the Michael receptor in PFPMD was the electrophilic warhead. Prior to docking, the force field of AMBER10: EHT and the implicit solvation model of Reaction Field (R-field) were selected. The docking workflow followed the “induced fit” protocol, in which the side chains of the receptor binding site was allowed to move according to ligand conformations, with a constraint on their positions. The

weight used for tethering side chain atoms to their original positions was 10. For the ligand, all docked poses of which were ranked by London dG scoring first, then a force field refinement was carried out on the top 30 poses followed by a rescoring of GBVI/WSA dG. The interactions complex protein-ligand conformations, including hydrogen bonds and the bond lengths were analyzed using PyMol.

6. Assessment of *KRAS*^{G12C} mutation in xenograft tissue.

Digital Polymerase Chain Reaction (dPCR) Analysis was used for verifying the *KRAS*^{G12C} mutation in xenograft tissue. Briefly, the tumor tissue was harvested for total RNA extraction using a UNIQ-10 column-Trizol extraction kit (Sangon Biotech, China) according to manufacturer's instruction. The primers were designed as following using Primer Premier 5.0 software. Reverse transcription was performed before dPCR. Microdroplet was prepared in 96-well plates (QX200, bio-rad, USA), then PCR amplification was started with the condition of (95°C, 10min; 94°C, 30s; 60°C, 1min, 98°C, 10min,40 cycles; 4°C, 10min), after that, the sample was analyzed using a microdroplet digital PCR instrument (QX200 Droplet, bio-rad, USA). Primer sequences were as follows: KRAS^{G12C}-F 5' AGGCCTGCTGAAAATGACTG 3', KRAS^{G12C}-R 5' TAGCTGTATCGTCAAGGCACTC3'.

7. Pharmacokinetics studies in male ICR mice and human.

Pharmacokinetics studies was executed as previously described. (Mol. Pharmaceutics **2023**, 20, 3, 1750–1757.) Fitting of different compartment models with different weighting factors were performed using the PKSlover pharmacokinetic program (*Comput. Meth. Programs Biomed.* **2010,** 99, (3), 306-314.) to screen for the best model.

SUPPLEMENTAL FIGURES

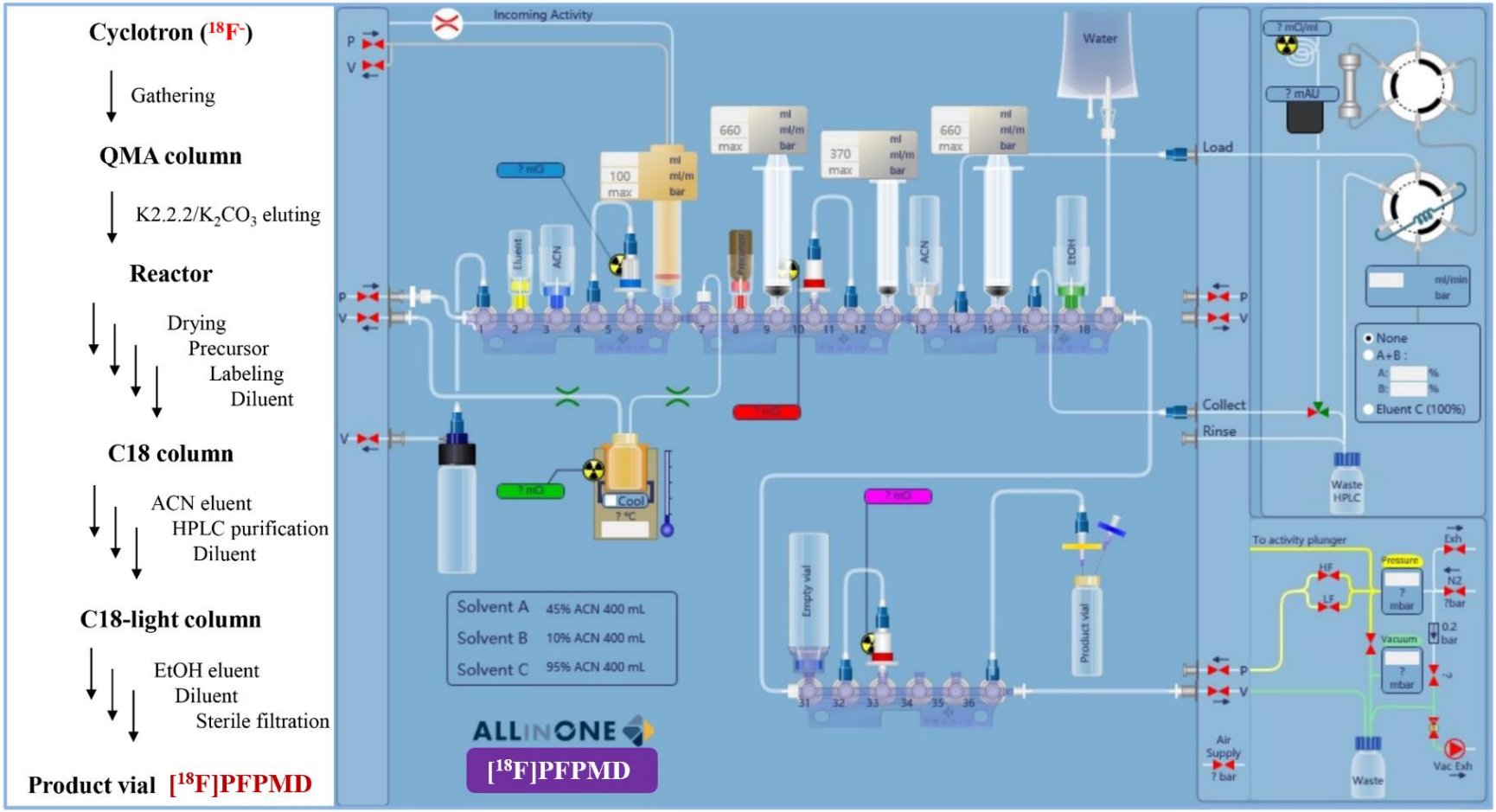

Supplemental Figure 1. Schematic diagram of the preparation of [^{18}F]PFPMD using the AllinOne universal synthesizer.

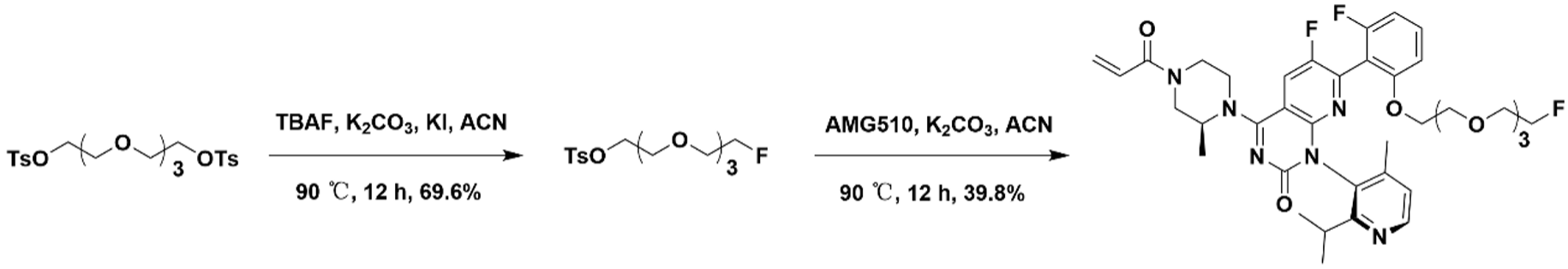

1 (OTs-PEG4-OTs) **2 (F-PEG4-OTs)** **PFPMD**

Supplemental Figure 2. The synthetic routes of nonradioactive PFPMD.

A

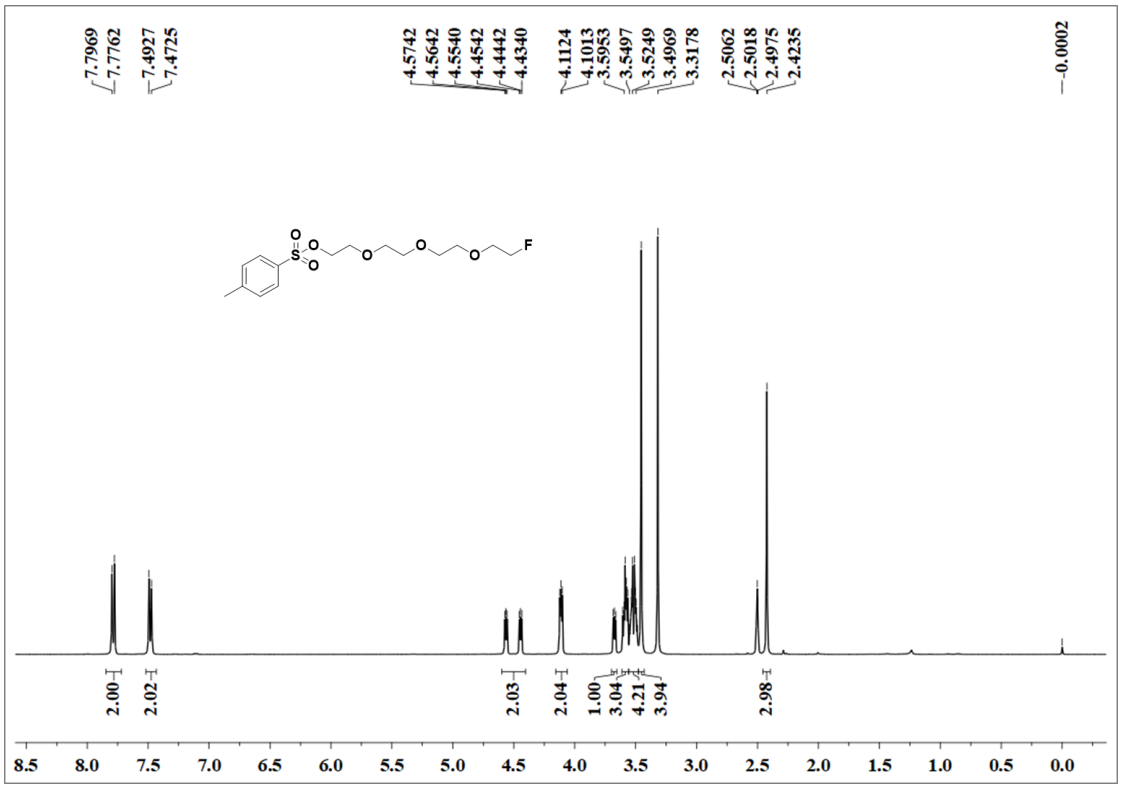
7.7969
7.7762
7.4927
7.4725
4.5742
4.5642
4.5540
4.4542
4.4442
4.4340
4.1124
4.1013
3.5953
3.5497
3.5249
3.4969
3.3178
2.5062
2.5018
2.4975
2.4235
0.0002
2.00
2.02
2.03
2.04
1.00
3.04
4.21
3.94
2.98
8.5 8.0 7.5 7.0 6.5 6.0 5.5 5.0 4.5 4.0 3.5 3.0 2.5 2.0 1.5 1.0 0.5 0.0

B

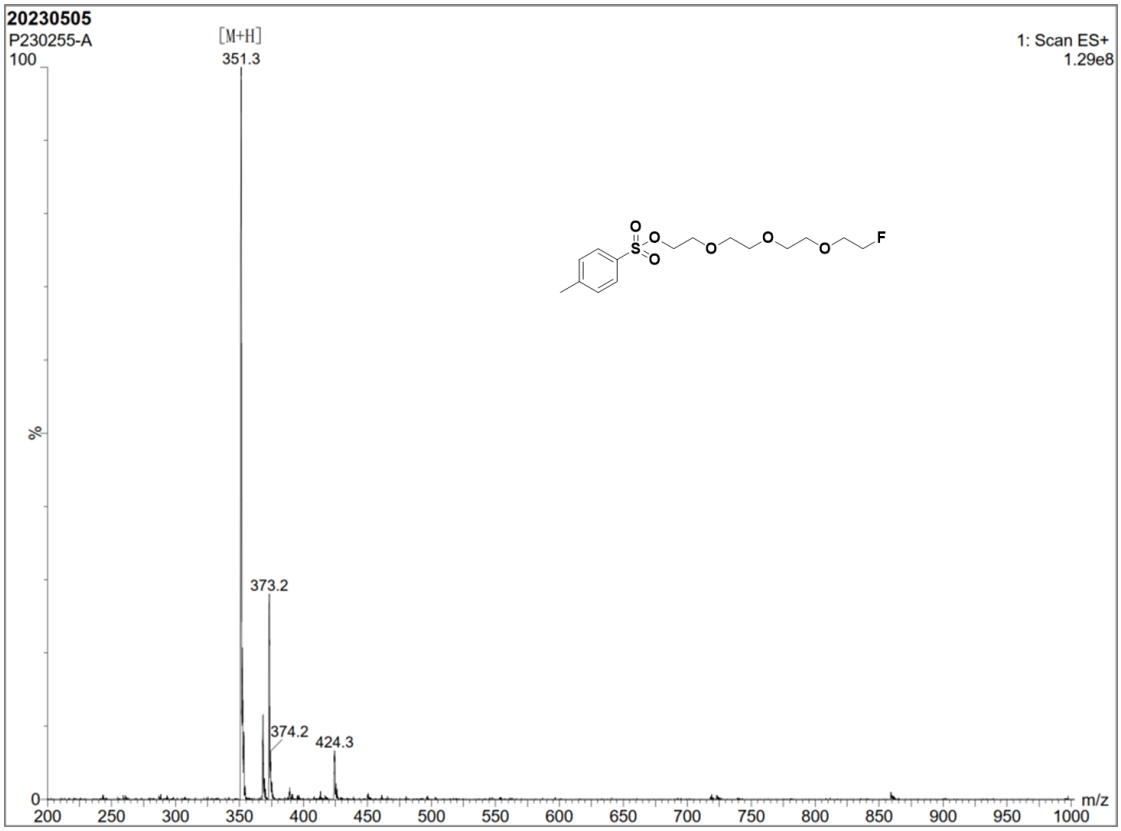
20230505
P230255-A
100
[M+H]
351.3
1: Scan ES+
1.29e8
%
373.2
374.2
424.3
0
200 250 300 350 400 450 500 550 600 650 700 750 800 850 900 950 1000
m/z

C

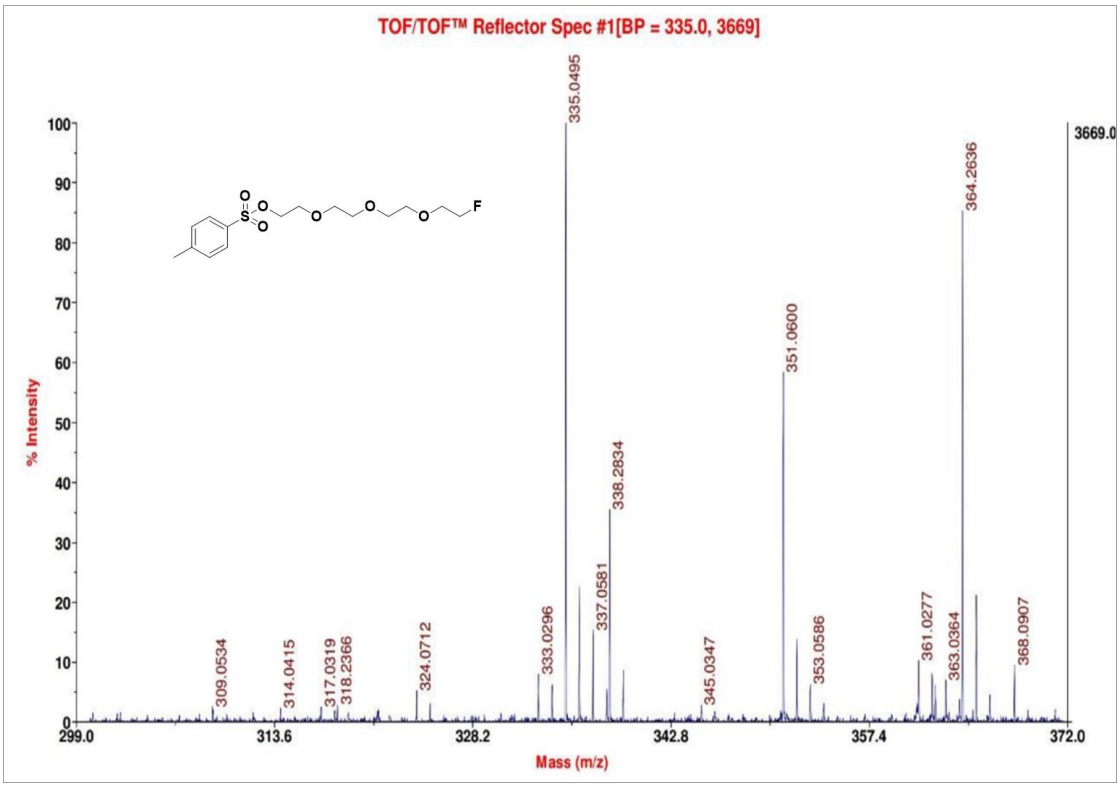

Supplemental Figure 3. Characterization of compound 2: *2-(2-(2-(2-fluoroethoxy)ethoxy)ethoxy)ethyl 4-methylbenzenesulfonate.* **(A)** H NMR (DMSO-d_6) spectrum; ^{1}H NMR (400 MHz, DMSO-d_6) δ (ppm): 7.79 (d, J = 8.3 Hz, 2H), 7.48 (d, J = 8.1 Hz, 2H), 4.60-4.40 (m, 2H), 4.11 (dd, J = 5.1, 3.7 Hz, 2H), 3.70-3.65 (m, 1H), 3.61-3.56 (m, 3H), 3.56-3.48 (m, 4H), 3.45 (s, 4H), 2.42 (s, 3H). **(B)** MS (ESI) spectrum; The 351.3 peak is the intermediate compound. MS(ESI), $[M + H]^+$: *m/z* = 351.3. **(C)** HRMS (ESI-Tof) spectrum; The 351.0600 peak is the intermediate compound. HRMS (ESI-Tof), $[M + H]^+$: *m/z* calculated for $C_{15}H_{24}FO_6S^+$ 351.1272, found 351.0600.

A

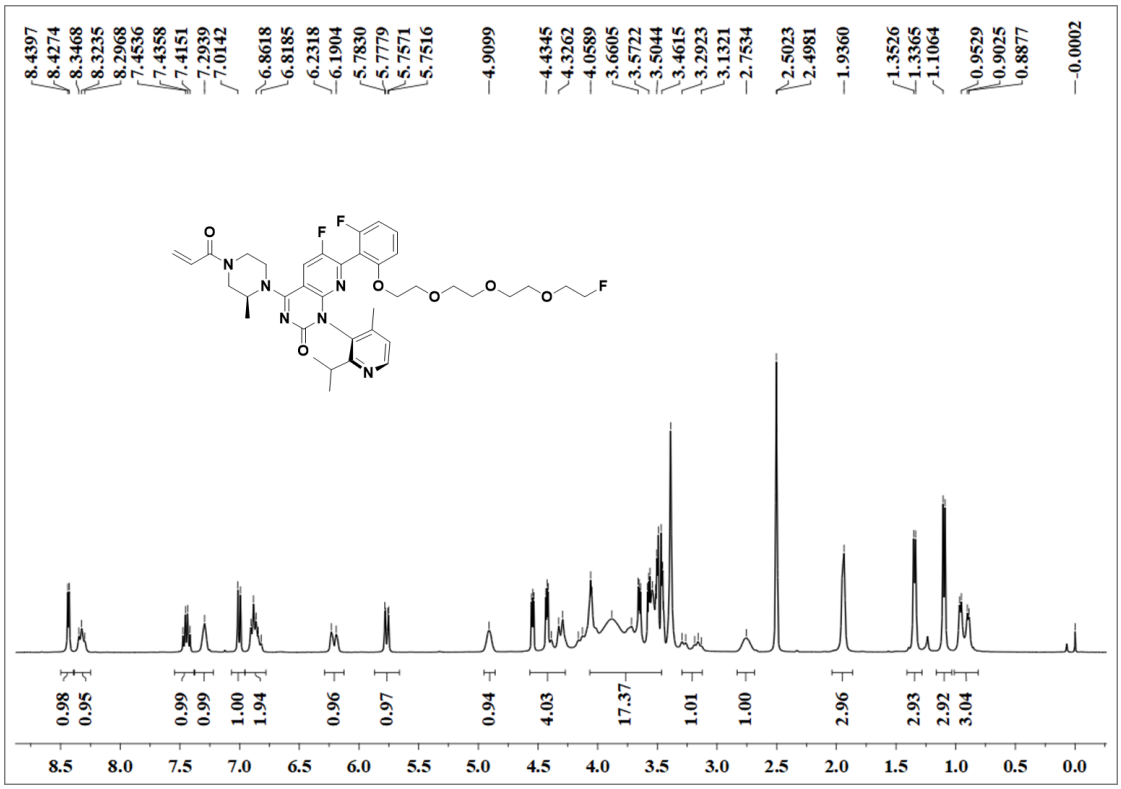
8.4397
8.4274
8.3468
8.3235
8.2968
7.4536
7.4358
7.4151
7.2939
7.0142
6.8618
6.8185
6.2318
6.1904
5.7830
5.7779
5.7571
5.7516
4.9099
4.4345
4.3262
4.0589
3.6605
3.5722
3.5044
3.4615
3.2923
3.1321
2.7534
2.5023
2.4981
1.9360
1.3526
1.3365
1.1064
0.9529
0.9025
0.8877
0.0002
0.98
0.95
0.99
0.99
1.00
1.94
0.96
0.97
0.94
4.03
17.37
1.01
1.00
2.96
2.93
2.92
3.04
8.5
8.0
7.5
7.0
6.5
6.0
5.5
5.0
4.5
4.0
3.5
3.0
2.5
2.0
1.5
1.0
0.5
0.0

B

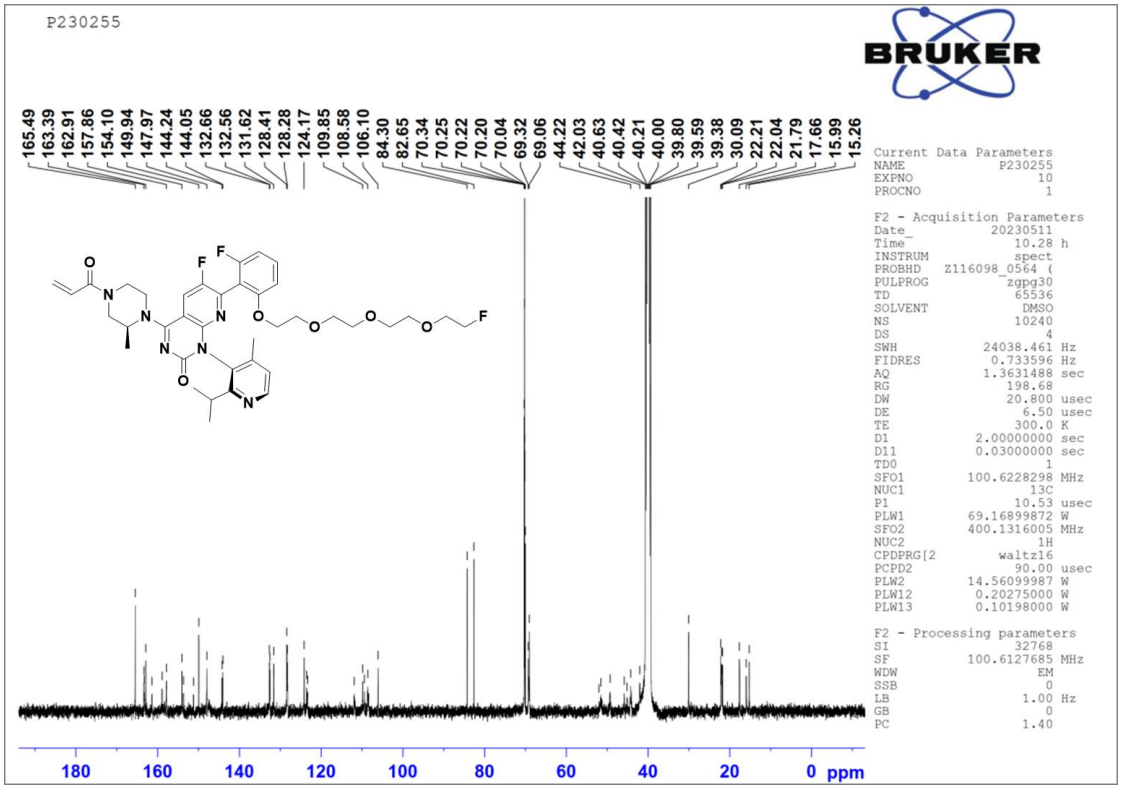
P230255
BRUKER
165.49
163.39
162.91
157.86
154.10
149.94
147.97
144.24
144.05
132.66
132.56
131.62
128.41
128.28
124.17
109.85
108.58
106.10
84.30
82.65
70.34
70.25
70.22
70.20
70.04
69.32
69.06
44.22
42.03
40.63
40.42
40.21
40.00
39.80
39.59
39.38
30.09
22.21
22.04
21.79
17.66
15.99
15.26
Current Data Parameters
NAME P230255
EXPNO 10
PROCNO 1
F2 - Acquisition Parameters
Date_ 20230511
Time 10.28 h
INSTRUM spect
PROBHD Z116098_0564 (
PULPROG zgpg30
TD 65536
SOLVENT DMSO
NS 10240
DS 4
SWH 24038.461 Hz
FIDRES 0.733596 Hz
AQ 1.3631488 sec
RG 198.68
DW 20.800 usec
DE 6.50 usec
TE 300.0 K
D1 2.00000000 sec
D11 0.03000000 sec
TD0 1
SFO1 100.6228298 MHz
NUC1 13C
P1 10.53 usec
PLW1 69.16899872 W
SFO2 400.1316005 MHz
NUC2 1H
CPDPRG[2 waltz16
PCPD2 90.00 usec
PLW2 14.56099987 W
PLW12 0.20275000 W
PLW13 0.10198000 W
F2 - Processing parameters
SI 32768
SF 100.6127685 MHz
WDW EM
SSB 0
LB 1.00 Hz
GB 0
PC 1.40
180
160
140
120
100
80
60
40
20
0 ppm

C

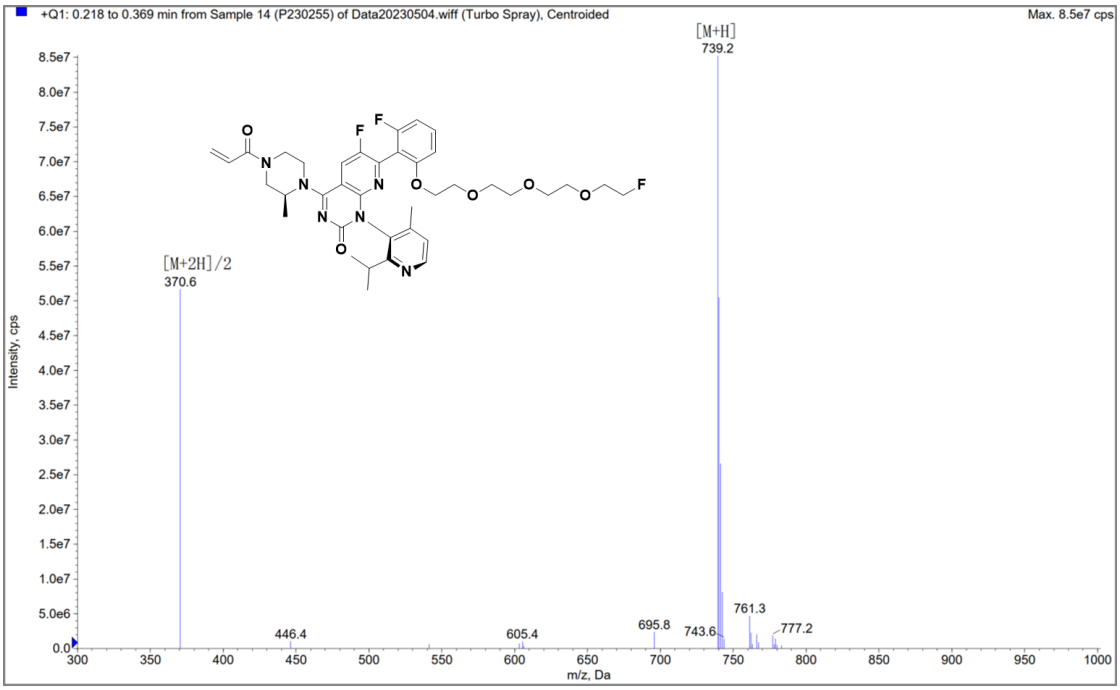

D

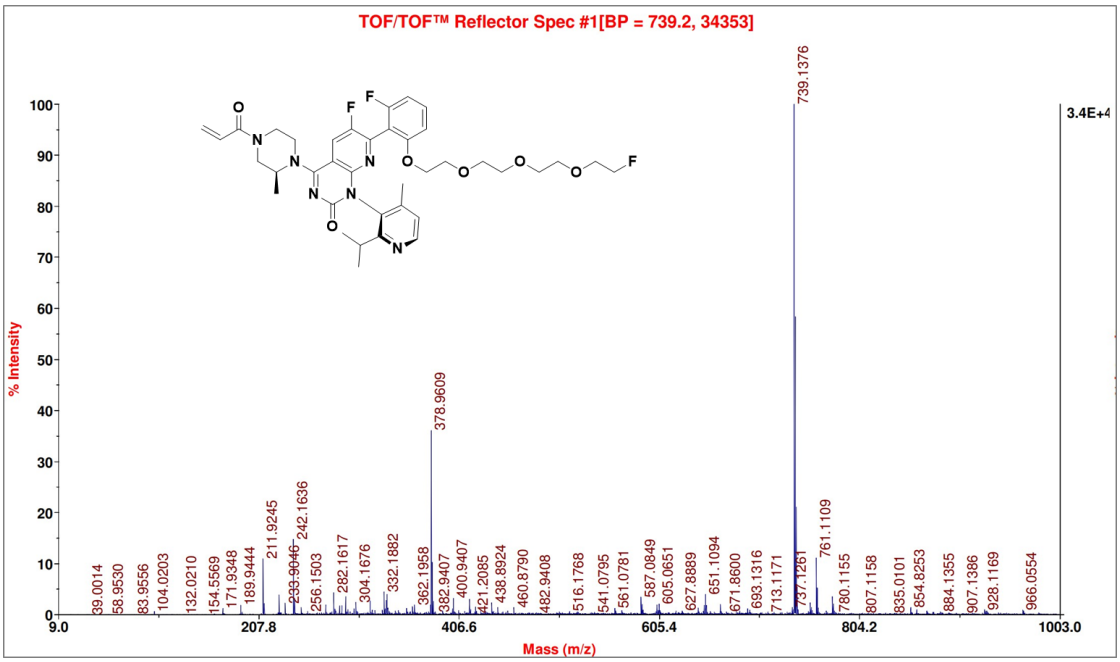

Supplemental Figure 4. Characterization of *4-((S)-4-acryloyl-2-methylpiperazin-1-yl)-6-fluoro-7-(2-fluoro-6-(2-(2-(2-(2-fluoroethoxy)ethoxy)ethoxy)ethoxy)phenyl)-1-(2-isopropyl-4-methylpyridin-3-yl)pyrido[2,3-d]pyrimidin-2(1H)-one (PFPMD)*: **(A)** H NMR (DMSO-d_6) spectrum; ^{1}H NMR (400 MHz, DMSO-d_6) δ (ppm): 8.43 (d, J = 4.9 Hz, 1H), 8.32 (t, J = 10.0 Hz, 1H), 7.44 (dd, J = 15.4, 8.3 Hz, 1H), 7.29 (s, 1H), 7.00 (d, J = 8.5 Hz, 1H), 6.95-6.78 (m, 2H), 6.21 (d, J = 16.5 Hz, 1H), 5.77 (dd, J = 10.4, 2.1

Hz, 1H), 4.91 (s, 1H), 4.57--3.46 (m, 21H), 3.29-3.12 (m, 1H), 2.75 (s, 1H), 1.94 (s, 3H), 1.34 (d, J = 6.4 Hz, 3H), 1.10 (d, J = 6.7 Hz, 3H), 0.93 (dd, J = 26.2, 6.1 Hz, 3H). **(B)** C NMR (DMSO-d_6) spectrum; ^{13}C NMR (101 MHz, DMSO-d_6) δ (ppm): 165.49, 163.39, 162.91, 157.86, 154.10, 149.94, 147.97, 144.24, 144.05, 132.66, 132.56, 131.62, 128.41, 128.29, 124.17, 109.85, 108.58, 106.10, 83.47 (d, J = 165.7 Hz, 1H), 70.34, 70.25, 70.22, 70.20, 70.04, 69.32, 69.06, 44.22, 42.03, 30.09, 22.21, 22.04, 21.79, 17.66, 15.99, 15.26. **(C)** MS (ES) spectrum; MS(ESI), $[M + H]^+$: m/z = 739.2. **(D)** HRMS (ESI-Tof) spectrum; HRMS (ESI-Tof), $[M + H]^+$: m/z calculated for $C_{38}H_{46}F_3N_6O_6^+$ 739.3425, found 739.1376.

A

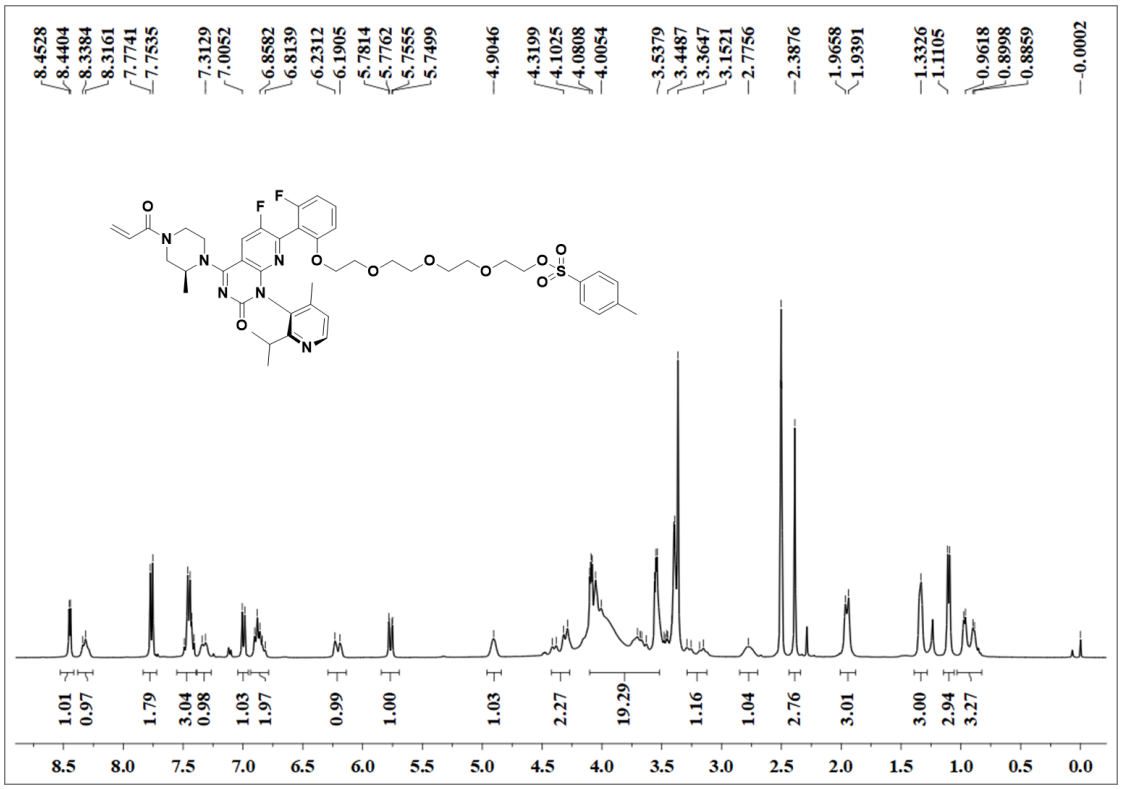
8.4528
8.4404
8.3384
8.3161
7.7741
7.7535
7.3129
7.0052
6.8582
6.8139
6.2312
6.1905
5.7814
5.7762
5.7555
5.7499
4.9046
4.3199
4.1025
4.0808
4.0054
3.5379
3.4487
3.3647
3.1521
2.7756
2.3876
1.9658
1.9391
1.3326
1.1105
0.9618
0.8998
0.8859
0.0002
1.01
0.97
1.79
3.04
0.98
1.03
1.97
0.99
1.00
1.03
2.27
19.29
1.16
1.04
2.76
3.01
3.00
2.94
3.27
8.5
8.0
7.5
7.0
6.5
6.0
5.5
5.0
4.5
4.0
3.5
3.0
2.5
2.0
1.5
1.0
0.5
0.0

B

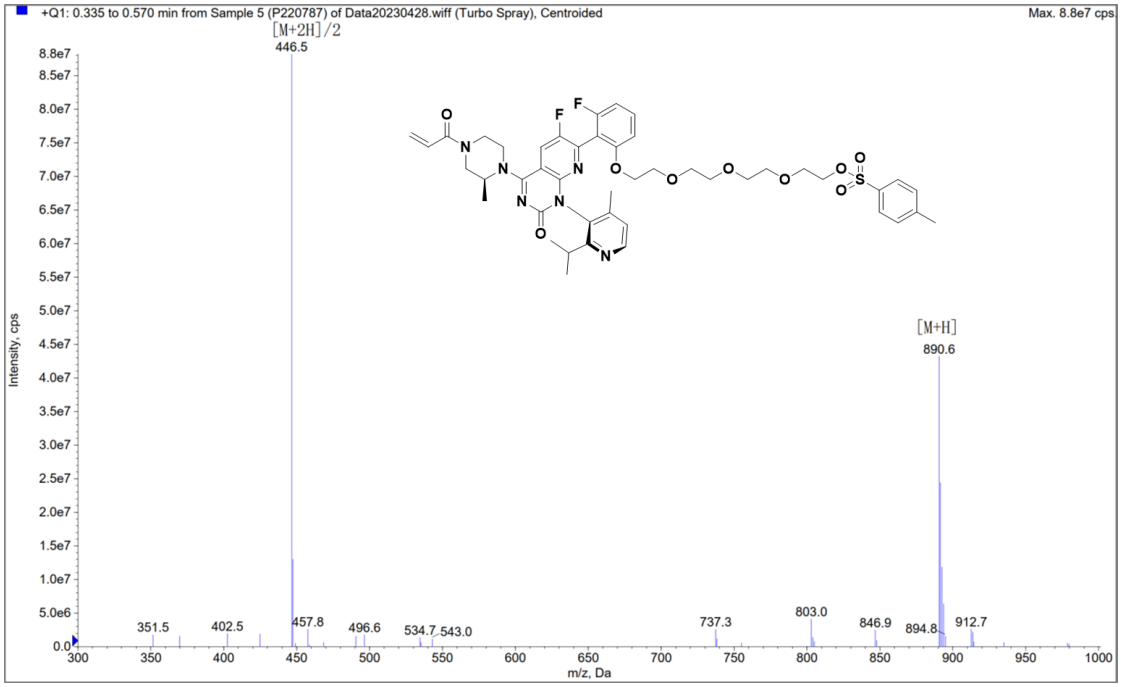
+Q1: 0.335 to 0.570 min from Sample 5 (P220787) of Data20230428.wiff (Turbo Spray), Centroided
Max. 8.8e7 cps
[M+2H]/2
446.5
[M+H]
890.6
Intensity, cps
m/z, Da
351.5
402.5
457.8
496.6
534.7
543.0
737.3
803.0
846.9
894.8
912.7

C

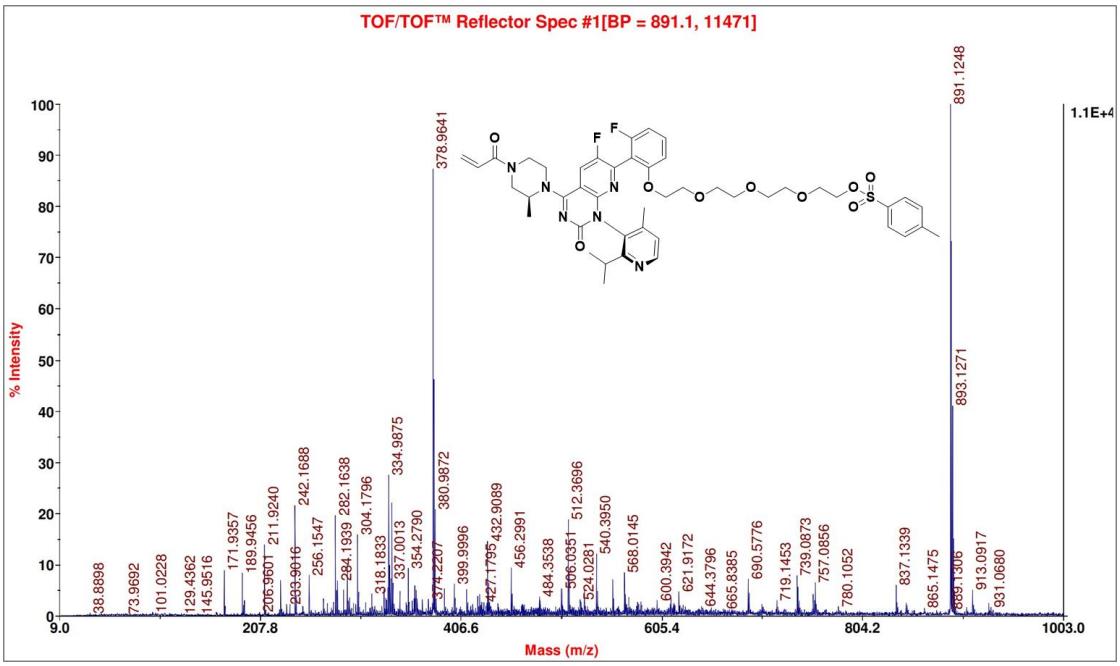

Supplemental Figure 5. Characterization of *2-(2-(2-(2-(2-(4-((S)-4-acryloyl-2-methylpiperazin-1-yl)-6-fluoro-1-(2-isopropyl-4-methylpyridin-3-yl)-2-oxo-1,2-dihydropyrido[2,3-d]pyrimidin-7-yl)-3-fluorophenoxy)ethoxy)ethoxy)ethoxy)ethyl 4-methylbenzenesulfonate (PPMD-OTs).* **(A)** ^{1}H NMR (400 MHz, DMSO-d_6) δ (ppm): 8.45 (d, *J* = 5.0 Hz, 1H), 8.33 (d, *J* = 8.9 Hz, 1H), 7.76 (d, *J* = 8.2 Hz, 2H), 7.55-7.39 (m, 3H), 7.33 (d, *J* = 10.8 Hz, 1H), 6.99 (d, *J* = 8.5 Hz, 1H), 6.94-6.78 (m, 2H), 6.21 (d, *J* = 16.3 Hz, 1H), 5.77 (dd, *J* = 10.4, 2.2 Hz, 1H), 4.90 (s, 1H), 4.42-4.27 (m, 2H), 4.10-3.52 (m, 19H), 3.29-3.12 (m, 1H), 2.78 (s, 1H), 2.39 (s, 3H), 1.95 (d, *J* = 10.7 Hz, 3H), 1.33 (s, 3H), 1.10 (d, *J* = 6.6 Hz, 3H), 0.93 (dd, *J* = 30.6, 5.8 Hz, 3H). **(B)** MS(ESI), $[M + H]^+$: *m/z* = 890.6. **(C)** HRMS (ESI-Tof) spectrum; HRMS (ESI-Tof), $[M + H]^+$: *m/z* calculated for $C_{45}H_{53}F_2N_6O_9S^+$ 891.3557, found 891.1248.

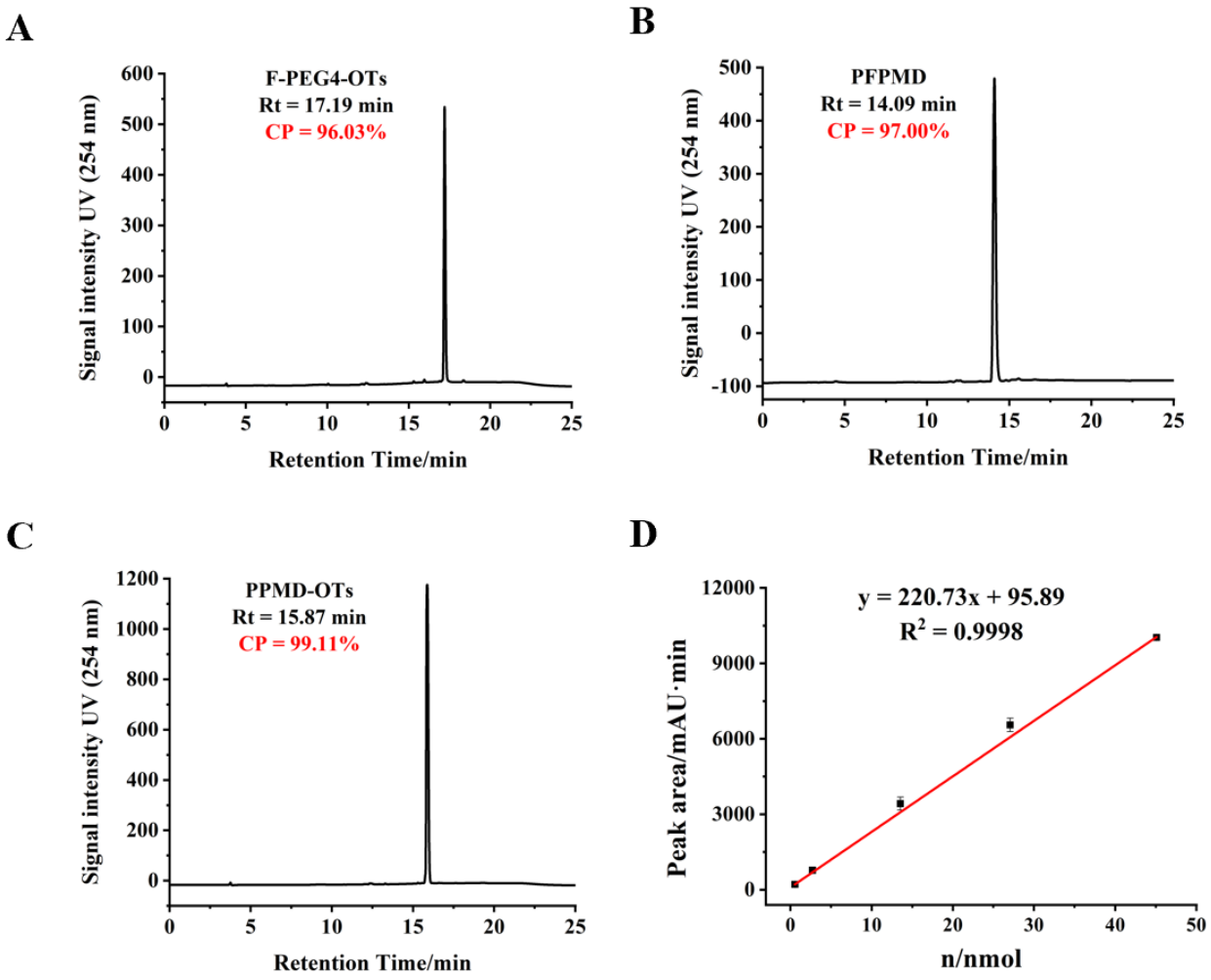

Supplemental Figure 6. HPLC confirmed the chemical purity of **(A)** F-PEG4-OTs, **(B)** PFPMD and **(C)** PPMD-OTs**. (D)** Standard curves of PFPMD.

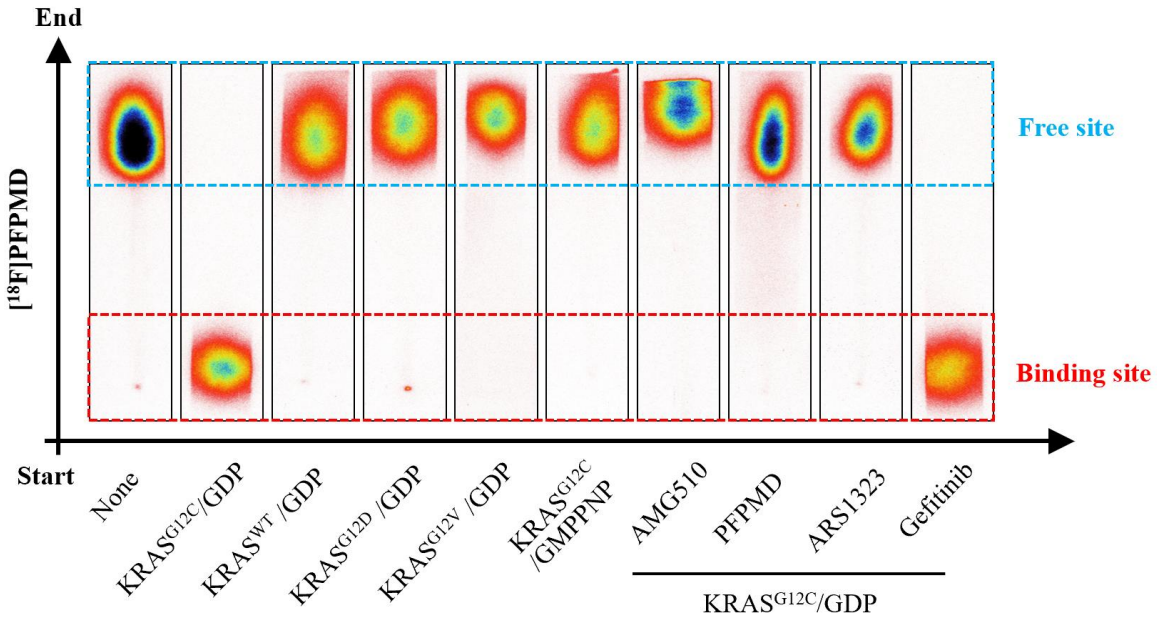

Supplemental Figure 7. Autoradiography of radio-TLC strips for determining the selectivity of [^{18}F]PFPMD toward KRAS^{G12C} oncoprotein. Once the tracer binds with protein, the binding site appeared radioactivity, while free tracers did not bind with protein would display at Free site. KRAS^{G12C}/GDP refers to KRAS^{G12C} oncoprotein coexist with GDP; GMPPNP, a GTP analogue; PFPMD, nonradioactive tracer; ARS1323, another KRAS^{G12C} inhibitor; Gefitinib, an EGFR-TKI.

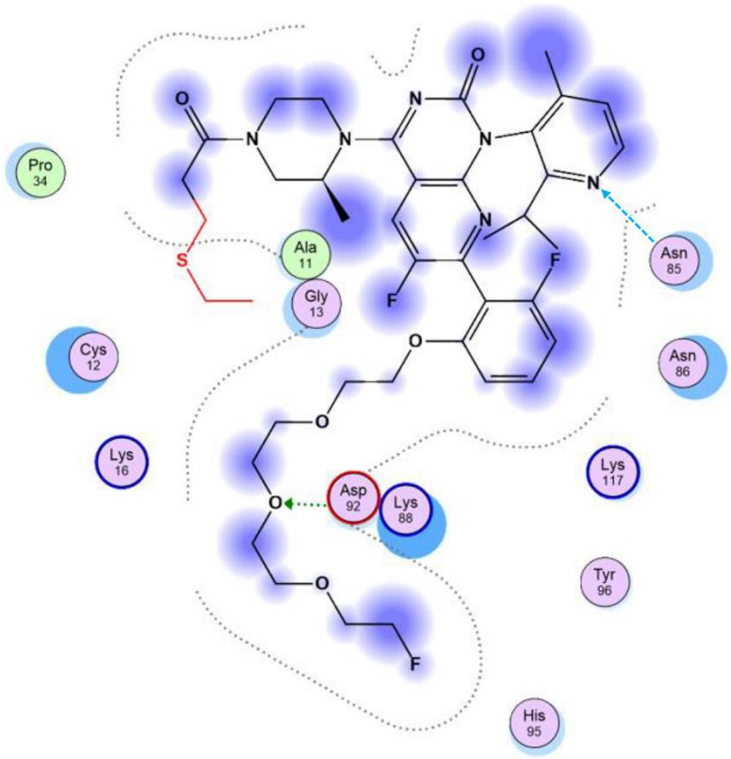

Supplemental Figure 8. Molecular docking revealed the complementarity of PFPMD to the binding site of KRAS^{G12C} protein. The acrylamide warhead of PFPMD forms a covalent bond with the sulfhydryl group of the cysteine residue through Michael's addition. As a hydrogen bond acceptor, the nitrogen atom of PFPMD formed a hydrogen bond with the hydrogen atom of Asn85 in KRAS^{G12C} (Blue dashed arrow). The oxygen atom of PFPMD, being also a hydrogen bond acceptor, formed a hydrogen bond with the hydrogen atom of Lys88 in KRAS^{G12C} (Green dashed arrow). Van Der Waals (VDW) interactions were also formed among PFPMD and the surrounding molecular residues. The binding energy of PFPMD and KRAS^{G12C} protein was -5.49 kcal/mol, which was similar to that of -5.11 kcal/mol between AMG510 and KRAS^{G12C} protein.

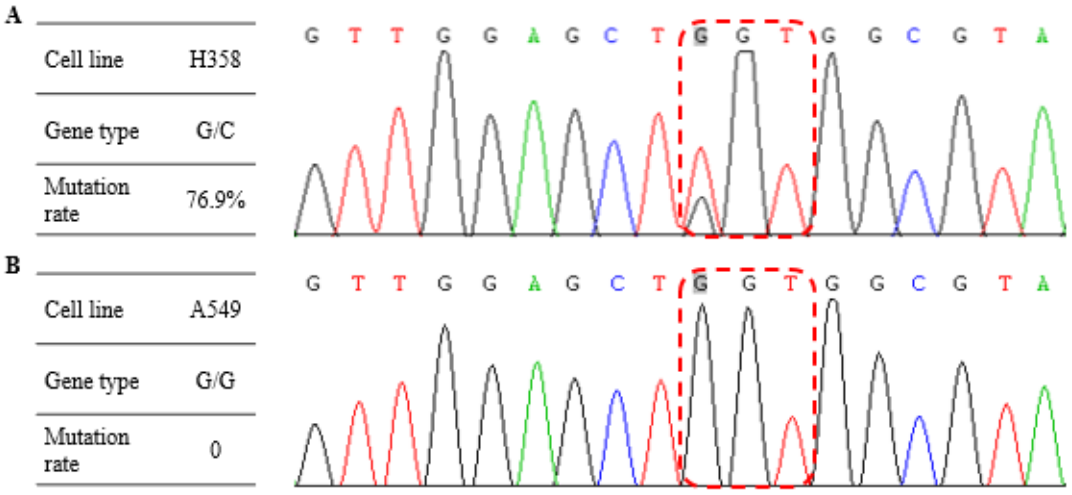

Supplemental Figure 9. Sanger sequencing for KRAS^{G12C} mutation in H358 and A549 cell line. **(A)** the KRAS mutation rate was 76.9% in H358 cell. **(B)** No KRAS mutation was detected in A549 cell line.

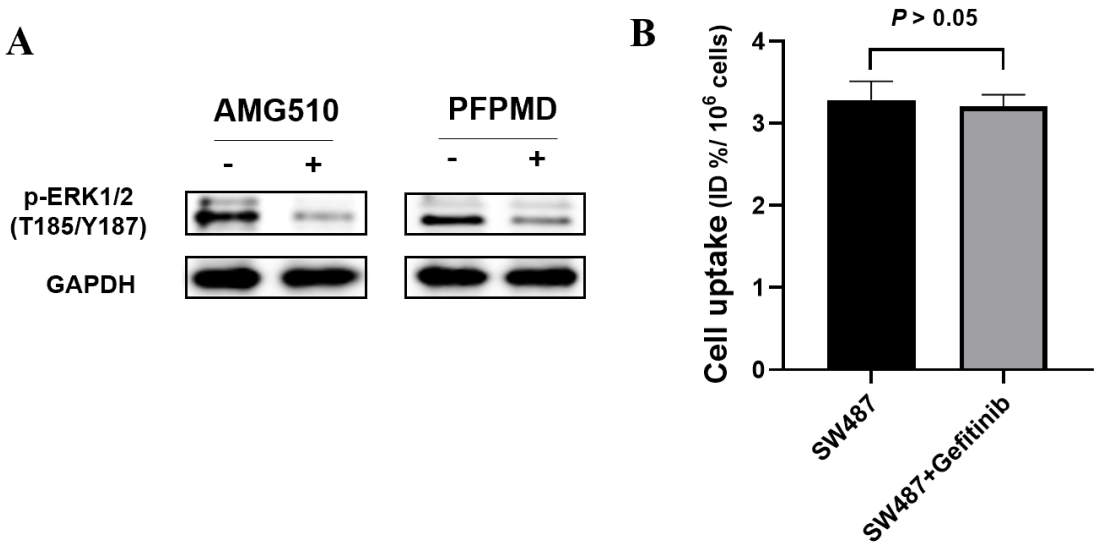

Supplemental Figure 10. (A) Western blot for assessment of the impact of AMG510 and PFPMD to downstream p-ERK expression in H358 cell line (n = 3). **(B)** [^{18}F]PFPMD uptake in SW837 cell line (KRAS^{G12C} mutation) and co-incubation with Gefitinib, an EGFR-TKI.

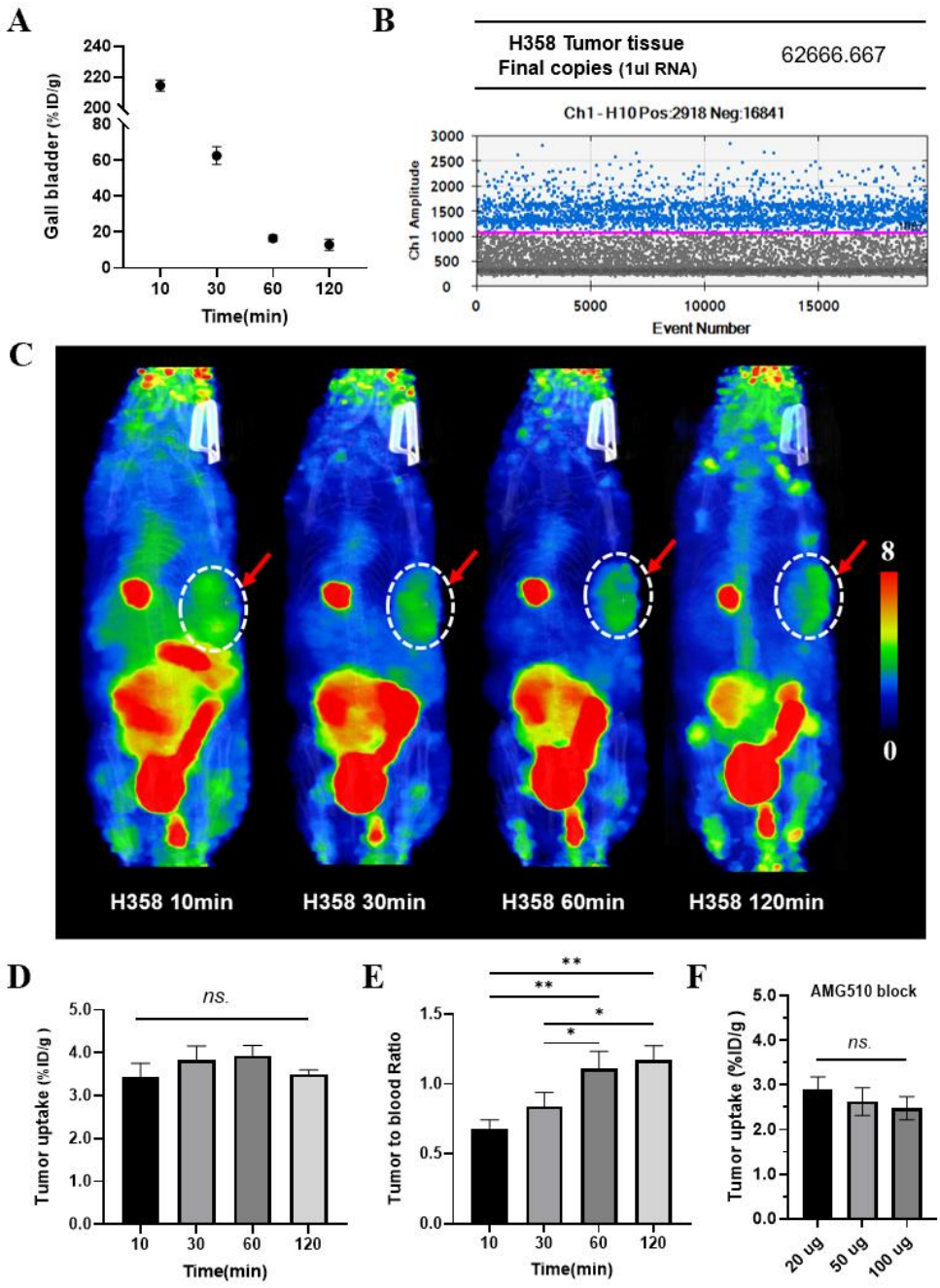

Supplemental Figure 11. (A) The accumulation of [^{18}F]PFPMD at gall bladder at different time points. (n = 3). **(B)** Digital PCR (dPCR) method for verifying the *KRAS*^{G12C} mutation in H358 xenograft tissue. **(C)** Dynamic [^{18}F]PFPMD PET/CT imaging in H358 tumor-bearing mice at 10 min, 30 min, 60 min and 120 min respectively (n = 3). **(D)** Tumor uptake of [^{18}F]PFPMD at indicated time points (n = 3). **(E)** Tumor to blood pool ratio at indicated time points. * $p < 0.05$, ** $p < 0.01$, (n = 3). **(F)** Tumor uptake of [^{18}F]PFPMD at different AMG510 blocking dosage (n = 5).

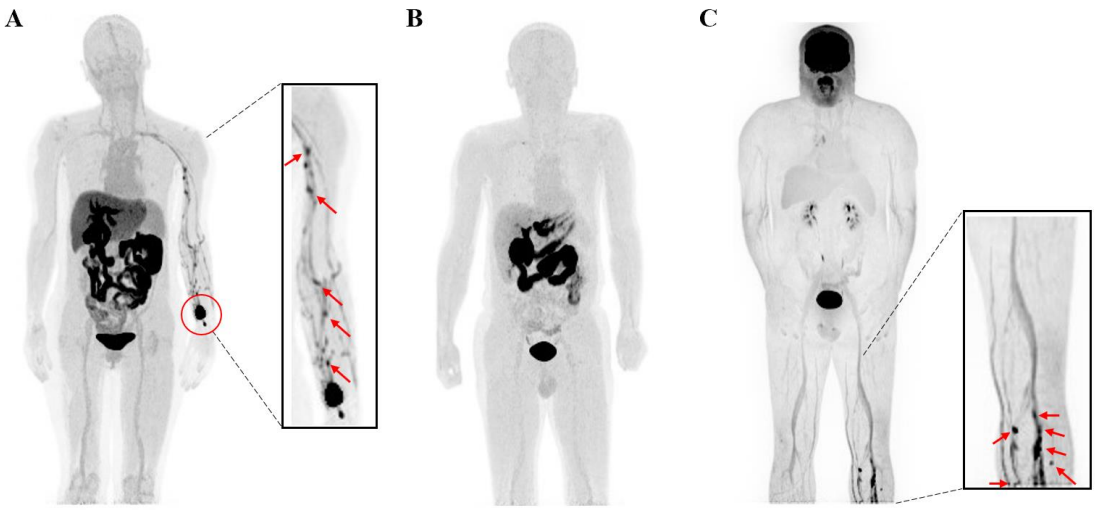

Supplemental Figure 12. (A) A 52 years old female volunteer whose [^{18}F]PFPMD PET image at 1 hour post injection showed tracer lingering in the vein and infiltration at the injection site. **(B)** A 55 years old male volunteer whose 1-hour [^{18}F]PFPMD PET image showed no tracer lingering in the veins. **(C)** A 36 years old patient whose [^{18}F]FDG PET image displayed tracer lingering in the vein of left leg.

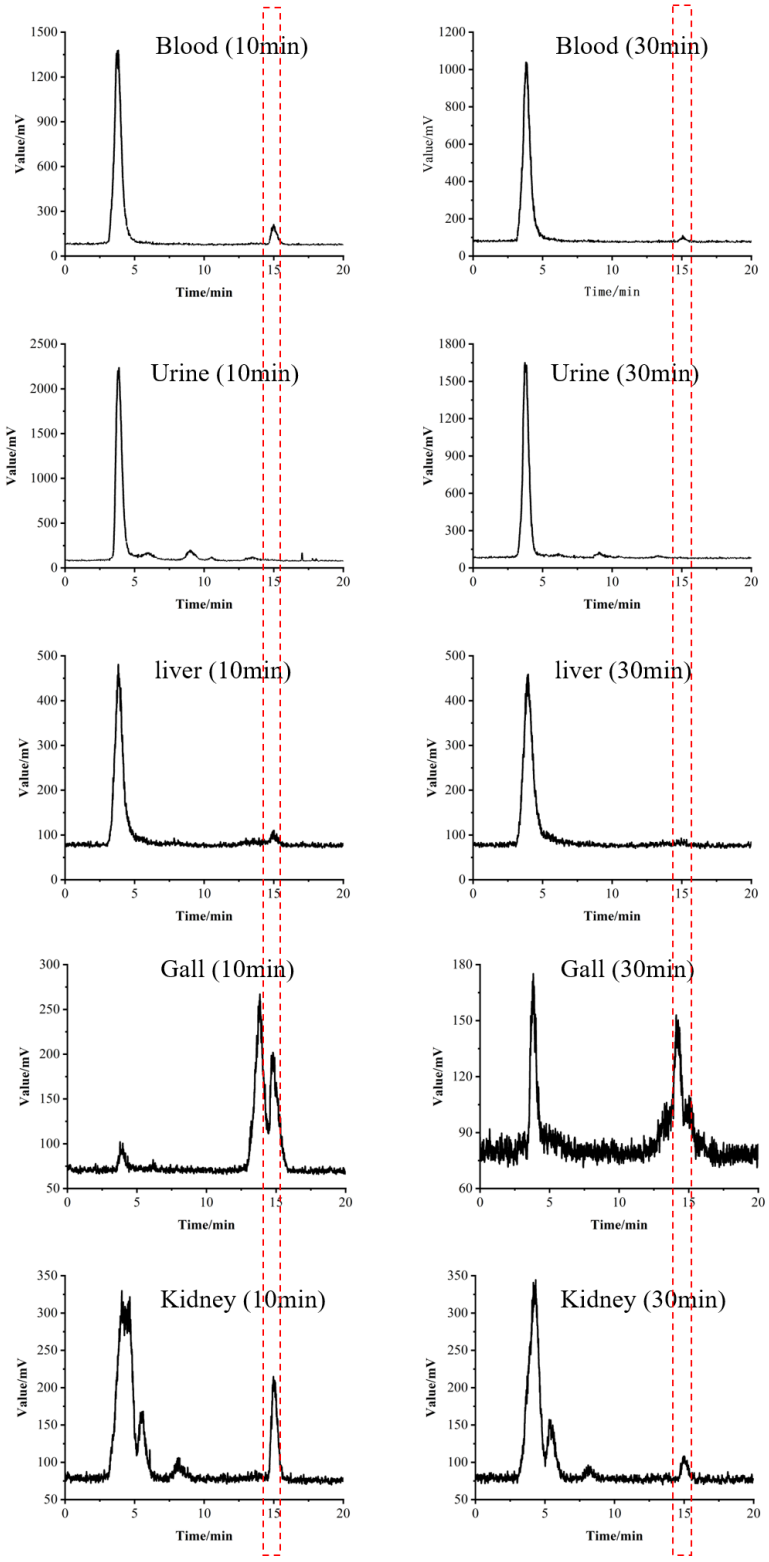

Supplemental Figure 13. The metabolic stability of [^{18}F]PFPMD *in vivo*. The *in vivo* metabolic stability of [^{18}F]PFPMD was analyzed in ICR mice using HPLC method by detecting the radioactive metabolites in blood, urine, liver, kidney and gall at 10 min and 30 min after p.i. administration.

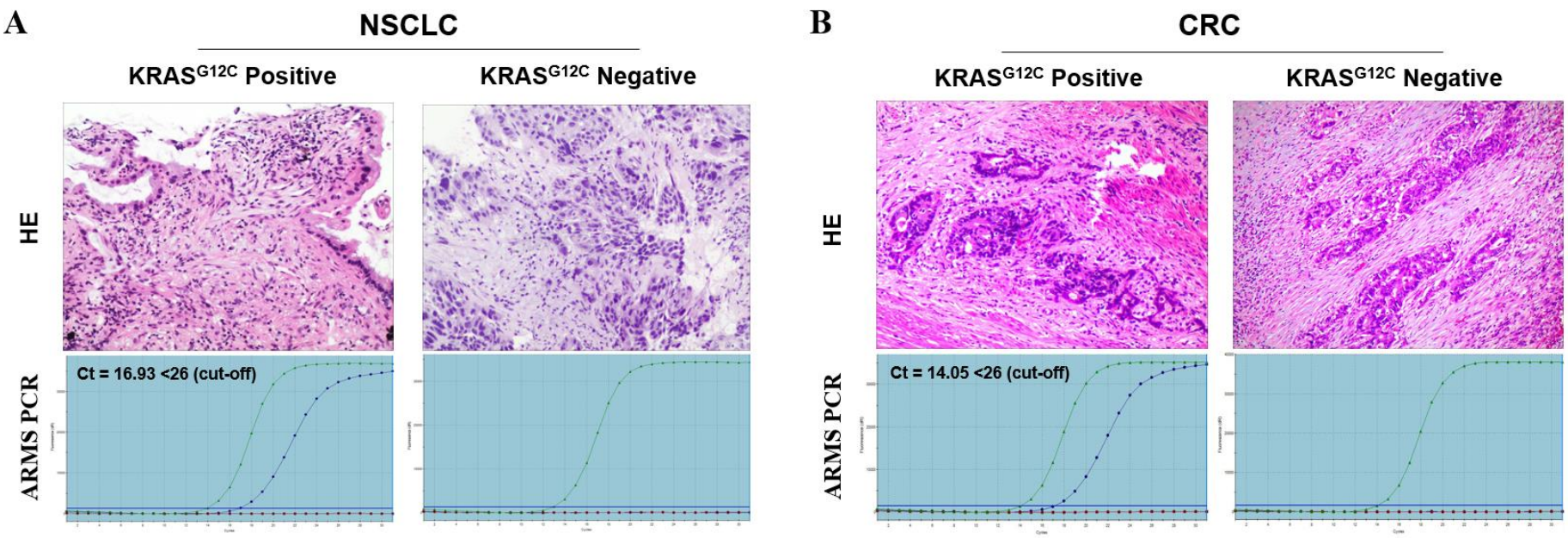

Supplemental Figure 14. Histology and AMRS PCR test for KRAS^{G12C} mutation in NSCLC and CRC patients. (A) Upper row, Hematoxylin-Eosin (HE) staining on KRAS^{G12C} positive and negative lung cancer tissues respectively. Lower row, AMRS PCR test results for determining KRAS^{G12C} mutation status in NSCLC patients. **(B)** Upper row, Hematoxylin-Eosin (HE) staining on KRAS^{G12C} positive and negative rectal cancer tissues respectively. Lower row, AMRS PCR test results for determining KRAS^{G12C} mutation status in CRC patients.

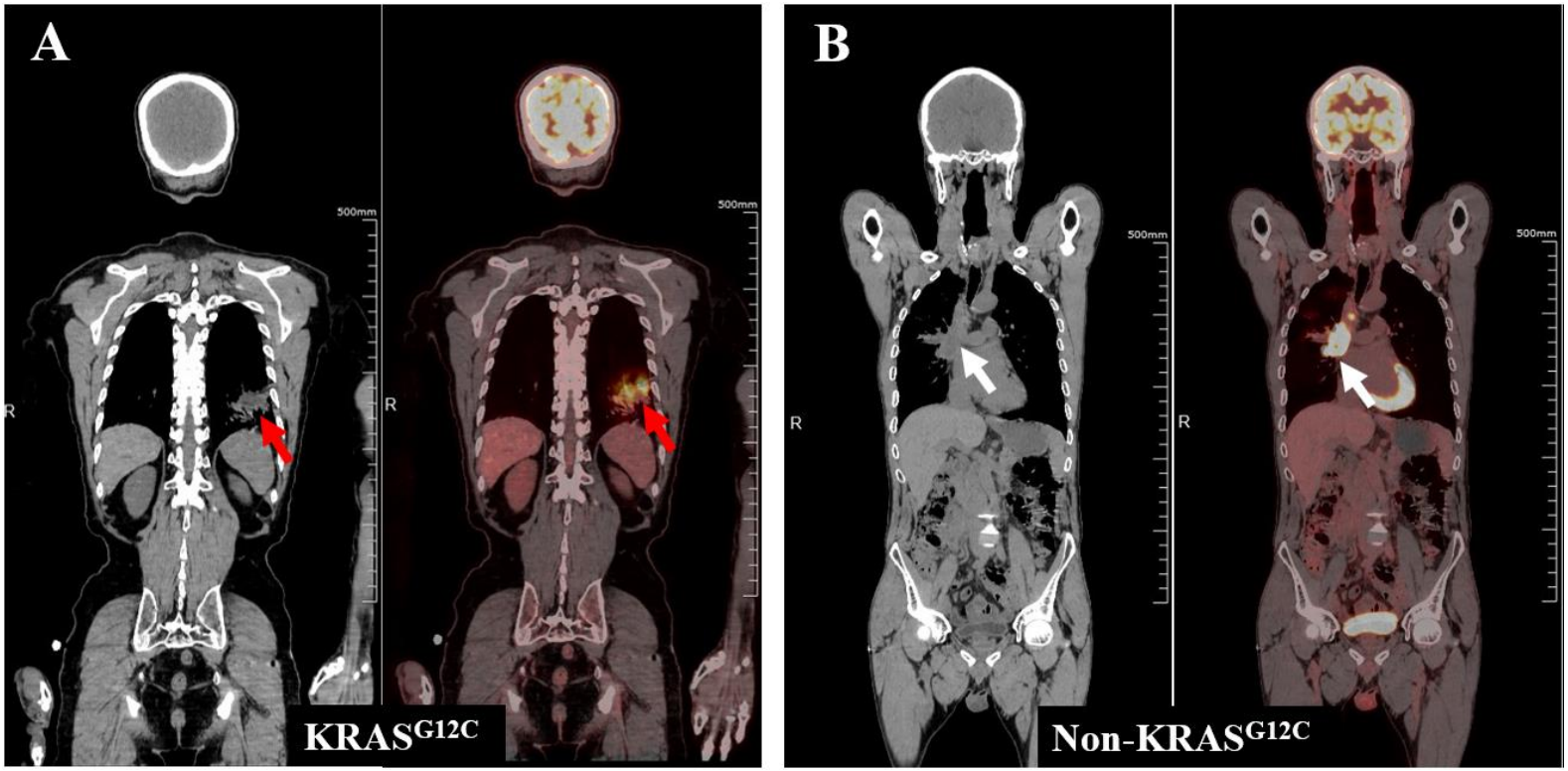

Supplemental Figure 15. Oncological [^{18}F]FDG PET/CT imaging in NSCLC patients. (A) Representative CT and [^{18}F]FDG PET/CT images of NSCLC patient with KRAS^{G12C} mutation. (B) Representative CT and [^{18}F]FDG PET/CT images of NSCLC patient without KRAS^{G12C} mutation.

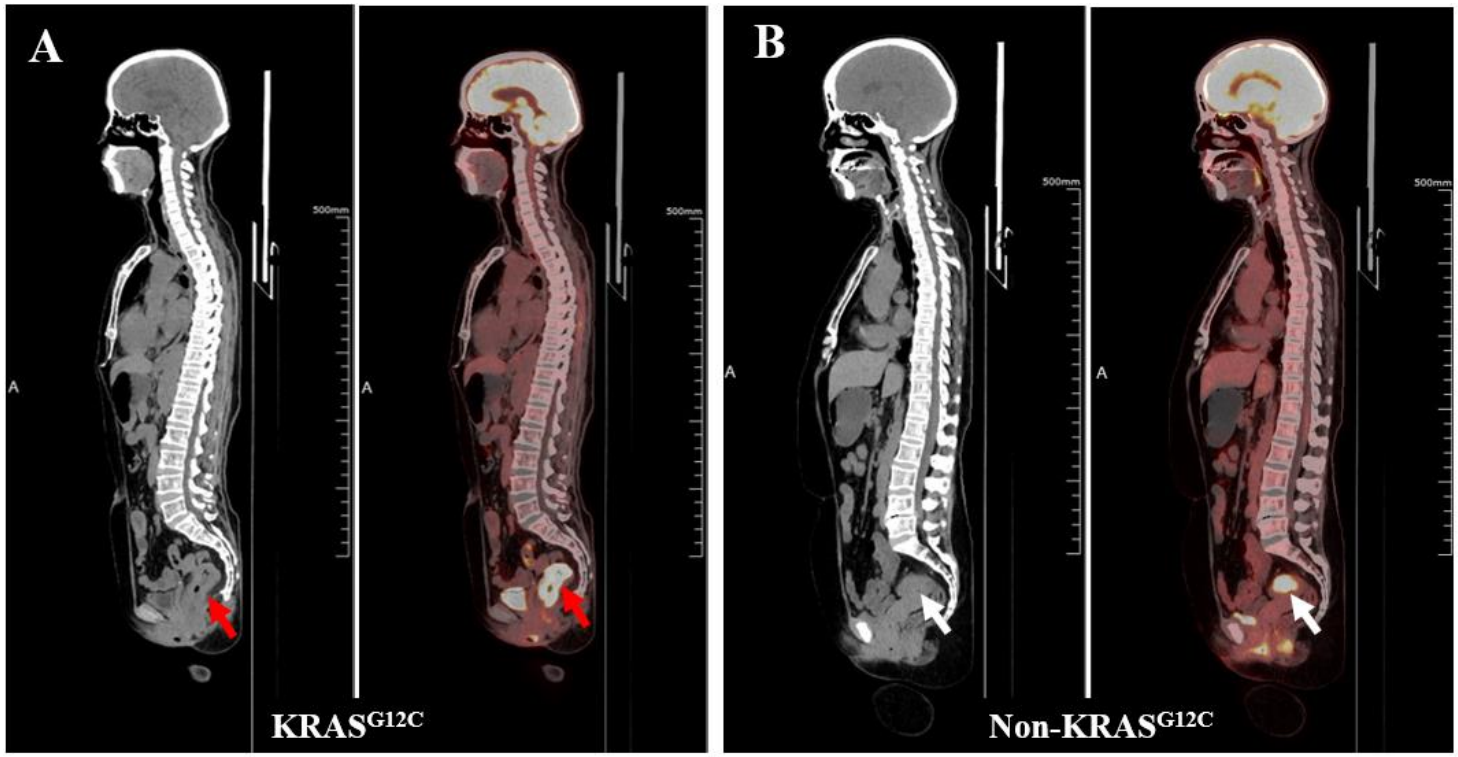

Supplemental Figure 16. Oncological [^{18}F]FDG PET/CT imaging in CRC patients. (A) Representative CT and [^{18}F]FDG PET/CT images of CRC patient with KRAS^{G12C} mutation. (B) Representative CT and [^{18}F]FDG PET/CT images of CRC patient without KRAS^{G12C} mutation.

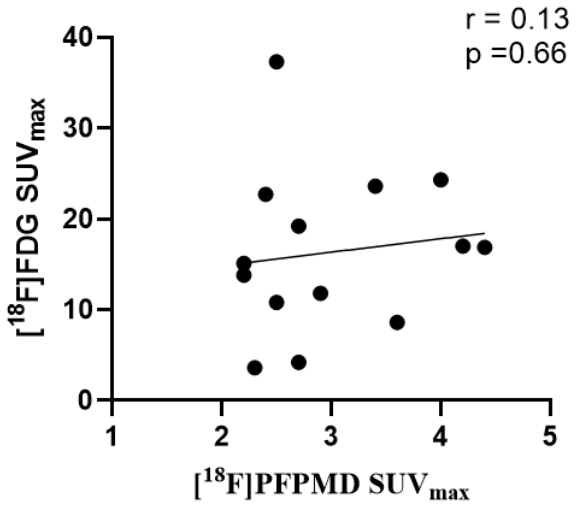

Supplemental Figure 17. The correlation of [^{18}F]FDG SUVmax and [^{18}F]PFPMD SUVmax in 14 NSCLC and CRC patients.

Supplemental Table 1. Demographic characteristics of the enrolled healthy volunteers.

Patient no.	Gender	Age (years)	Weight (kg)	Hight (cm)	^{18}F-AMG510 Dose (MBq)
1	Female	52	59	167	192.96
2	Male	43	60	168	193.14
3	Male	55	65	172	185.37
4	Female	56	63	156	243.31
5	Male	68	60	165	330.48

Supplemental Table 2. *ex vivo* Biodistribution of [^{18}F]PFPMD in healthy male ICR mice (n = 3 for each timepoint).

	Percent injected dose per gram (%ID/g)				
Tissue	5 min	15 min	30 min	60 min	120 min
Blood	6.05 ± 0.47	5.09 ± 0.24	4.82 ± 0.31	3.70 ± 0.60	2.94 ± 0.32
Brain	3.37 ± 0.10	3.59 ± 0.09	2.85 ± 0.17	2.38 ± 0.52	2.02 ± 0.31
Heart	5.19 ± 0.37	4.37 ± 0.33	4.69 ± 0.51	4.06 ± 0.57	2.79 ± 0.47
Liver	5.78 ± 0.52	4.07 ± 0.40	3.58 ± 0.29	2.52 ± 0.82	2.05 ± 0.35
Spleen	4.30 ± 0.21	3.96 ± 0.14	3.26 ± 0.71	2.78 ± 0.65	2.24 ± 0.33
Lungs	5.47 ± 0.16	4.29 ± 0.49	3.98 ± 0.48	3.10 ± 0.55	2.44 ± 0.29
Kidneys	7.20 ± 0.20	4.80 ± 0.27	4.15 ± 0.73	3.13 ± 0.49	2.30 ± 0.30
Small intestine	8.24 ± 2.85	7.22 ± 4.37	5.13 ± 1.22	3.82 ± 0.90	2.63 ± 0.61
Large intestine	3.37 ± 0.94	5.20 ± 0.22	8.33 ±1.68	12.61 ±2.36	12.53 ±0.70
Stomach	3.50 ± 0.47	3.44 ± 0.50	2.87 ± 0.46	2.28 ± 0.30	1.62 ± 0.27
Muscle	3.52 ± 0.35	3.52 ± 0.28	3.10 ± 0.18	2.41 ± 0.51	1.95 ± 0.36
Bone	2.10 ± 0.21	2.29 ± 0.32	2.91 ± 1.34	4.18 ± 0.95	4.15 ± 1.26

Supplemental Table 3. *ex vivo* Biodistribution of [^{18}F]PFPMD in tumor-bearing BALB/c nude mice at 1 hour post injection (n=5 for each group).

Percent injected dose per gram (%ID/g)					
Tissue	H358	A549	H358+20 μg AMG510	H358+50 μg AMG510	H358+100 μg AMG510
Tumor	3.93 ± 0.24	2.47 ± 0.26	2.89 ± 0.29	2.63 ± 0.31	2.48 ± 0.26
Blood	3.14 ± 1.1	3.18 ± 0.18	3.13 ± 0.41	2.91 ± 0.26	2.82 ± 0.12
Brain	2.18 ± 0.87	2.04 ± 0.1	1.93 ± 0.3	1.72 ± 0.39	1.88 ± 0.22
Heart	2.83 ± 0.73	3.11 ± 0.14	2.56 ± 0.29	2.35 ± 0.13	2.51 ± 0.1
Liver	2.23 ± 1.18	1.61 ± 0.39	2.09 ± 0.44	1.94 ± 0.21	2.6 ± 0.57
Spleen	2.17 ± 0.82	1.78 ± 0.22	2.02 ± 0.26	1.86 ± 0.27	2.27 ± 0.35
Lungs	2.22 ± 0.7	2.33 ± 0.28	2.32 ± 0.62	2.36 ± 0.36	2.23 ± 0.25
Kidneys	2.08 ± 0.72	2.35 ± 0.11	3.83 ± 2.99	2.19 ± 0.76	1.95 ± 0.27
Small intestine	4.3 ± 3.19	10.85 ± 6.63	2.38 ± 0.25	2.59 ± 0.29	10.07 ± 4.34
Large intestine	11.95 ± 2.14	13.61 ± 1.54	12.29 ± 1.16	12.06 ± 1.90	14.17 ± 1.17
Stomach	3.21 ± 1.11	2.31 ± 0.32	1.92 ± 0.26	1.83 ± 0.13	3.02 ± 1.27
Muscle	2.16 ± 0.72	1.94 ± 0.19	2.11 ± 0.49	1.61 ± 0.28	1.95 ± 0.18
Bone	2.72 ± 0.68	3.58 ± 1.12	1.78 ± 0.13	2.07 ± 0.16	1.63 ± 0.31

Supplemental Table 4. Rationale for selection of hemodynamic chamber model

	Modle	Diagnostics	Weight		
			1	1/c	1/cc
Mice	1 Compartment	r obs-pre	0.9957	0.9948	0.9943
		SS	0.1962	0.2327	0.2870
		WSS	0.1962	0.0576	0.0165
		R^2	0.9976	0.9971	0.9964
		WR^2	0.9976	0.9993	0.9998
		SE	0.2215	0.1200	0.0642
		AIC	-5.7713	-13.1267	-20.6287
		SC	-6.1878	-13.5432	-21.0452
	2 Compartment	r obs-pre	0.9990	0.9990	0.9990
		SS	0.0445	0.0454	0.0452
		WSS	0.0445	0.0177	0.0080
		R^2	0.9994	0.9994	0.9994
		WR^2	0.9994	0.9998	0.9999
		SE	0.1491	0.0940	0.0632
		AIC	-10.6766	-16.2154	-20.9762
		SC	-11.5096	-17.0484	-21.8092
Human	1 Compartment	r obs-pre	0.9849	0.9701	0.9435
		SS	0.0000	0.0001	0.0002
		WSS	0.0000	0.0030	0.2135
		R^2	0.9846	0.9733	0.9117
		WR^2	0.9846	-0.2393	-86.3804
		SE	0.0031	0.0275	0.2310
		AIC	-57.1328	-30.7989	-5.2644
		SC	-57.5492	-31.2153	-5.6809
	2 Compartment	r obs-pre	0.9995	0.9991	0.9984
		SS	0.0000	0.0000	0.0000
		WSS	0.0000	0.0001	0.0089
		R^2	0.9995	0.9992	0.9986
		WR^2	0.9995	0.9446	-2.6509
		SE	0.0007	0.0082	0.0668
		AIC	-74.2928	-45.4417	-20.3162
		SC	-75.1257	-46.2747	-21.1492

Supplemental Table 5. Pharmacokinetic behavior of [^{18}F]PFPMD.

Parameter	Mice		Human	
	Unit	Value	Unit	Value
k10	1/min	0.0324	1/min	0.0179
k12	1/min	0.326	1/min	0.0378
k21	1/min	0.206	1/min	0.0419
t1/2α	min	1.25	min	7.76
t1/2β	min	57.3	min	82.4
C0	% ID/g	15.5	‰ ID/ml	0.0634
V	(MBq)/(% ID/g)	0.0478	(mCi)/(‰ ID/ml)	94.6
CL	(MBq)/(% ID/g)/min	0.00150	(mCi)/(‰ ID/ml)/min	1.69
V2	(MBq)/(% ID/g)	0.0756	(mCi)/(‰ ID/ml)	85.3
CL2	(MBq)/(% ID/g)/min	0.0156	(mCi)/(‰ ID/ml)/min	3.58
AUC 0-t	% ID/g*min	452	‰ ID/ml*min	3.49
AUC 0-inf	% ID/g*min	478	‰ ID/ml*min	3.54
AUMC	% ID/g*min^2	38000	‰ ID/ml*min^2	377
MRT	min	79.6	min	106
Vss	MBq/(% ID/g)	0.123	mCi/(‰ ID/ml)	180

For mice. The basis for the selection of the hemodynamic atrial model was calculated by the PKSlover pharmacokinetic program. Supplemental Table 4 showed that both the values of Akaike information criterion (AIC) and Schwartz criterion (SC) were minimal for the two-compartment model at a weighting factor of 1/cc, thus, this model was most consistent with the *in vivo* metabolism of [^{18}F]PFPMD. The blood concentration reached the highest level rapidly after the tail vein injection, the distribution half-life ($T_{1/2}\alpha$) was 1.26 min and the clearance half-life ($T_{1/2}\beta$) was 57.3 min. For human. By the PKSlover pharmacokinetic program, we also calculated that the two-compartment model at a weighting factor of 1, which was most consistent with the *in vivo* metabolism of [^{18}F]PFPMD in human (Figure 3C and Supplemental Table 5). [^{18}F]PFPMD was more slowly distributed ($T_{1/2}\alpha$ = 7.76 min) and cleared ($T_{1/2}\beta$ = 82.4 min) from the body in humans than in mice.